MTOR as a selectable genomic harbor for CRISPR-engineered CAR-T cell therapy

Sébastien Levesque[1,2,3], Gillian Carleton[4,5], Victoria Duque[1,2], Claudia Goupil[1,2], Jean-Philippe Fiset[1,2], Sarah Villeneuve[1,2], Eric Normandeau[6], Geneviève Morin[6], Nellie Dumont[7], Josée Laganière[7], Brian Boyle[6], Julian J. Lum[4,5], Yannick Doyon[1,2*]

[1]Centre Hospitalier Universitaire de Québec Research Center - Université Laval, Québec, QC, G1V 4G2, Canada.
[2]Université Laval Cancer Research Centre, Québec, QC, G1V 0A6, Canada.
[3]Present Address: Division of Hematology/Oncology, Boston Children's Hospital. Department of Pediatric Oncology, Dana-Farber Cancer Institute. Harvard Stem Cell Institute. Broad Institute of MIT and Harvard. Department of Pediatrics, Harvard Medical School, Boston, MA 02115, USA.
[4]Trev and Joyce Deeley Research Centre, BC Cancer, Victoria, BC, V8R 6V5, Canada.
[5]Department of Biochemistry and Microbiology, University of Victoria, Victoria, BC, V8P 5C2, Canada.
[6]Institut de Biologie Intégrative des Systèmes, Université Laval, Québec, QC, G1V 0A6.
[7]Medical Affairs and Innovation, Héma-Québec, Québec, Quebec, Canada

[*]Correspondence:
Yannick Doyon, Ph.D.
Centre de recherche du CHU de Québec – Université Laval
2705, boulevard Laurier, T-3-67
Québec, QC G1V 4G2
CANADA

Tel: 418-525-4444 ext. 46264
e-mail: Yannick.Doyon@crchudequebec.ulaval.ca
ORCID 0000-0002-3889-9563

ABSTRACT

Chimeric antigen receptors (CARs) reprogram T cells to recognize and target cancer cells. Despite remarkable responses observed with CAR-T cell therapy in patients with hematological malignancies, CAR-T cell engineering still relies mostly on randomly integrating vectors, limiting the possibilities of fine-tuning T cell function. Here, we designed a CRISPR-based marker-free selection strategy to simultaneously target a therapeutic transgene and a gain-of-function mutation to the *MTOR* locus to enrich cells resistant to rapamycin, a clinically used immunosuppressant. We readily engineered rapamycin-resistant (RapaR) CAR-T cells by targeting CAR expression cassettes to the *MTOR* locus. Using *in vitro* cytotoxicity assays, and a humanized mouse model of acute lymphoblastic leukemia, we show that RapaR-CAR-T cells can efficiently target CD19^{+} leukemia cells in presence of rapamycin. Furthermore, our strategy allows multiplexed targeting of rapamycin-regulated immunoreceptors complexes (DARICs) to the *MTOR* and *TRAC* loci to pharmacologically control CAR-T cells' activity. We foresee that our approach could both facilitate the enrichment of CRISPR-engineered CAR-T cells *ex vivo* and *in vivo* while improving tumor eradication.

INTRODUCTION

Adoptive cell therapy with chimeric antigen receptor T (CAR-T) cells has shown remarkable potency against relapsed and refractory acute lymphoblastic leukemia (ALL) and non-Hodgkin lymphoma[1–5]. CAR-T cells are genetically engineered T cells that are able to recognize and target cancer cells expressing a specific antigen on their surface[6,7]. Randomly integrating vectors based on retroviruses, lentiviruses or *piggyBac* transposons are routinely used for cell therapy applications, but genome editing technologies offer a wide a range of opportunities to enhance CAR-T cells functionality[8,9]. The promising potential of CRISPR-based technologies to engineer CAR-T cells has been demonstrated by targeting a CAR to the *TRAC* locus to avert tonic CAR signaling and delay T cells differentiation and exhaustion[10], or by generating HLA-independent T cell receptors (HIT) to afford high antigen sensitivity[11]. CRISPR-based technologies also offer great potential to inactivate key genes involved in T cells dysfunction[12–14] or to generate allogeneic universal CAR-T cells[15–17].

While progress has been made towards high-yield targeted transgene integration in primary cells[10,11,18], enrichment strategies could further facilitate the development of CRISPR-engineered cell therapies. To enrich targeted transgene integration via homology-directed repair (HDR) in primary T cells, a selection method based on the expression of a methotrexate-resistant dihydrofolate reductase mutant has previously been reported[19]. A metabolic safety switch has also been developed via *UMPS* knockout to enrich T cells expressing reporter transgenes[20]. However, no marker-free selection strategy has been developed to simultaneously enrich CRISPR-engineered CAR-T cells and enhance their antitumor activity.

The serine/threonine protein kinase mTOR constitutes the catalytic subunit of two distinct complexes, known as mTORC1 and mTORC2, which coordinate eukaryotic cell growth and metabolism by integrating a diverse set of environmental inputs[21–23]. mTORC1 controls cellular growth and metabolism by sensing nutrient levels and growth factor signals to coordinate anabolic and catabolic metabolism[24]. While mTORC1 is sensitive to rapamycin, an immunosuppressant also used in oncology, mTORC2 remains functional upon acute rapamycin treatment[21–23]. Considering that mTOR signaling is commonly activated in tumor cells and alters the expression and the activity of key metabolic enzymes[21,25,26], combinatorial CAR-T cell therapy with rapamycin could synergistically enhance antitumor activity. Indeed, random integration of a rapamycin-resistant mTOR transgene and a CD19-CAR in primary T cells using *piggyBac* transposons has been shown to confer a selective growth advantage in the presence of rapamycin and enhanced antitumor activity when used in combination[27]. However, delivery of this large transgene is limiting, and product-derived lymphomas have been reported with *piggyBac*-modified CAR-T cells[28,29], so editing the endogenous *MTOR* locus to generate dominant cellular resistance to rapamycin using CRISPR could be a viable alternative. Since mTORC1 signaling lies downstream of several activation signals essential for T cell activation and expansion[21,30], this central signaling node is a prime target to develop a tissue-specific marker-free selection strategy for CRISPR-engineered CAR-T cells.

In this study, we performed saturation prime editing[31] at the *MTOR* locus to identify and characterize optimal mutations conferring rapamycin resistance. We then devised an intron nesting strategy[32,33] to enrich CRISPR-engineered cells *ex vivo* and *in vivo* without using an exogenous

94 selection marker. We demonstrate that targeting CAR expression cassettes to the *MTOR* locus
95 allows the selection and regulation of rapamycin-resistant CAR-T cells to perform combinatorial
96 immunotherapy with rapamycin. More broadly, we propose a versatile approach to facilitate
97 targeted therapeutic transgene integration for cell therapy applications.
98

99 # RESULTS

100 **Identification and characterization of mutations conferring rapamycin resistance via**
101 **saturation prime editing**

102 After an extraordinary 18-month response to everolimus, a rapamycin analog, a patient with
103 metastatic anaplastic thyroid carcinoma relapsed with a resistant tumor harboring the *MTOR*-
104 F2108L mutation[34]. The same mutation was also found in spontaneous rapamycin-resistant yeast
105 mutants[35], and a clonal MCF-7 breast cancer cell line after three months of exposure to
106 rapamycin[36]. Of importance, this mutation does not hyperactivate mTOR[32,34,36] and confers
107 resistance to first-generation allosteric inhibitors of mTOR, but not to second- and third-generation
108 inhibitors[34,36]. F2108 lies within the FKBP12-rapamycin binding (FRB) domain of mTOR and is
109 an important residue involved in rapamycin interactions[37]. We performed saturation mutagenesis
110 of F2108 to install all possible amino acids substitutions at the endogenous *MTOR* locus to identify
111 and characterize alternative mutations causing rapamycin-resistance at this position. We devised
112 a saturation prime editing (PE) screen[31] using K562 cells stably expressing the mScarlet-I mTOR
113 signaling indicator (mSc-TOSI)[32,38] as a phenotypic readout to interrogate the functional impact of
114 these mutations (**Fig. 1a,b** and **Supplementary Fig. 1**). Under active mTORC1 signaling, the
115 fluorescent mSc-TOSI reporter is rapidly phosphorylated by S6K, ubiquitinated, and degraded by
116 the proteasome while mTOR inhibition stabilizes the reporter (**Fig. 1b**)[32,38].
117

118 We transfected our reporter cell line with a library of engineered pegRNA (epegRNA)[39] encoding
119 F2108 variants and performed rapamycin selection starting 3 days post-transfection until all non-
120 resistant cells were eliminated. Selection was performed at 0.5 μM rapamycin, the lowest
121 concentration of this drug that strongly abrogates K562 cell proliferation under our growth
122 conditions. We performed high-throughput sequencing prior and after FACS-based cell sorting
123 and analyzed the fold enrichment of all possible *MTOR*-F2108 permutations (**Fig. 1c,d** and
124 **Supplementary Fig. 1**). The most enriched mutation was F2108L[34,36] (4.8 fold enrichment), but

125 five additional mutations displaying 1.6 to 2.3 fold enrichments were selected for further
126 characterization (**Fig. 1d**). Of importance, cells modified at *MTOR* remained sensitive to the 2nd
127 generation ATP-competitive inhibitor AZD8055[40], which could be used as a safety switch in case
128 of overt toxicity (**Fig. 1c** and **Supplementary Fig. 1** and **2**).
129
130 To validate the top hits, we designed epegRNAs to test these variants individually. K562 cells
131 harboring these *MTOR*-F2108 substitutions grew robustly in the presence of 0.5 μM rapamycin
132 and we observed a marked increase in the percentage of alleles harboring the PE-specified edits
133 after rapamycin selection (**Supplementary Fig. 1**). As expected, no resistance and no enrichment
134 were observed with the silent F2108F mutation (**Supplementary Fig. 1**). These observations
135 confirmed that the five new variants identified by saturation prime editing conferred dominant
136 cellular resistance to rapamycin. Furthermore, mTORC1 signaling remained fully functional with
137 the F2108L mutation but was completely blocked with the silent F2108F mutation
138 (**Supplementary Fig. 1 and 2**). However, intermediate levels of signaling in the presence of
139 rapamycin were observed with F2108I, F2108M, and F2108G while weak activity observed with
140 F2108V and F2108K (**Supplementary Fig. 1 and 2**). These observations suggest that robust K562
141 cell growth can be maintained with partial mTORC1 signaling. These *MTOR*-F2108 mutations
142 could potentially be used to pharmacologically fine-tune mTORC1 signaling while maintaining
143 robust cellular growth. Overall, mTORC1 signaling remains completely functional in the presence
144 of rapamycin with F2108L, and this mutation was selected to develop a marker-free selection
145 strategy to engineer rapamycin-resistant CAR-T cells.
146
147 **Concomitant transgene integration and induction of rapamycin resistance by nuclease-**
148 **driven *MTOR* editing in primary T cells.**
149 While creating F2108L by itself via PE could be used to potentiate CAR-T cells, we aimed to
150 determine if we could couple rapamycin resistance to transgene integration in a single step by
151 editing the *MTOR* locus via homology-directed repair (HDR). As we previously showed for the
152 essential *ATP1A1* gene[32], this strategy can work by nesting a transgene within an intron without
153 disrupting the recipient gene[32,33]. We first designed two sgRNAs targeting *MTOR* intron 45 in
154 proximity to F2108 using CRISPOR[41] (see G4 and G5 in **Fig. 1a**). These two chemically modified
155 sgRNAs generated 86-90% indels in primary T cells when delivered as RNPs with both SpCas9

156 and the high-fidelity variant HiFiCas9[42] (**Fig. 2a**). To assess their genome-wide specificity, we
157 performed GUIDE-Seq[43,44] in primary CD3$^+$ T cells from two healthy donors using wild-type
158 SpCas9. While 9 potential off-target sites were identified with *MTOR*-G5, only one was identified
159 with *MTOR*-G4 in CD3$^+$ T cells (**Fig. 2b** and **Supplementary Fig. 3**). Similar results were
160 obtained in K562 cells via plasmid overexpression (**Supplementary Fig. 3**). Since *MTOR*-G4 is
161 highly active with the HiFiCas9 variant, we prioritized this sgRNA for our studies.
162
163 Next, using Cas9 RNPs and PCR-generated linear dsDNA donors[45], we confirmed that rapamycin
164 resistance could be achieved in primary CD3$^+$ T cells and observed a marked increase to up to
165 62% of alleles harboring the *MTOR*-F2108L mutation after selection (**Supplementary Fig. 4**).
166 This increase in HDR in the population upon selection was concomitant with a decrease of indels
167 detected at the cut site, suggesting efficient elimination of cells not having undergone HDR
168 (**Supplementary Fig. 4**). No enrichment was observed when using a donor that harbored the
169 wildtype *MTOR*-F2108 codon, confirming that robust growth in the presence of rapamycin
170 depends on the *MTOR*-F2108L mutation (**Supplementary Fig. 4**). In these experiments, a dose of
171 25 nM rapamycin was chosen based on growth curves indicating that maximal inhibition occurred
172 in the 16-32 nM range under our conditions (data not shown). A similar dose was used in previous
173 studies[27] and it falls between the immunosuppressive window of 3-22 nM and the maximal steady-
174 state plasma drug concentrations observed in clinical settings[46,47]. Thus, the installation of the well-
175 characterized *MTOR*-F2108L mutation[34,36] via HDR confers dominant cellular resistance to
176 rapamycin in primary T cells.
177
178 We then devised the strategy to simultaneously target a therapeutic transgene and introduce the
179 F2108L mutation to the *MTOR* locus (**Fig. 3a**). After targeted integration, *MTOR*-F2108L is
180 expressed on the forward DNA strand while the moderately active human *PGK1* promoter drives
181 the expression of a therapeutic transgene of interest on the reverse DNA strand (**Fig. 3a**). As a first
182 test, we targeted an expression cassette encoding the fluorescent protein mScarlet-I to the *MTOR*
183 locus in CD3$^+$ T cells using linear dsDNA donors[45]. Rapamycin selection reproducibly doubled
184 targeted integration frequency and we observed up to 31% of cells expressing the nested reporter
185 transgene (**Supplementary Fig. 5**). Similarly, we achieved 11% knock-in efficacy of a CD19-
186 CAR-2A-EGFP gene cassette (4.6 kb) following treatment for 8 days with rapamycin

187 (**Supplementary Fig. 6**). While encouraging, the use of large linear dsDNA donor caused toxicity,
188 limited proliferation, and was generally prohibitive for highly efficient gene targeting[45]. In
189 addition, these experiments were performed with $CD3^+$ T cells retained in leukoreduction system
190 (LRS) chambers that are typically discarded by blood banks. We found that these cells have higher
191 death rates and limited growth potential under our genome editing conditions in contrast to cells
192 isolated from whole blood donations. Nevertheless, taken together, these data illustrate that
193 rapamycin resistant primary T cells can be engineered to express transgenes in a single homology-
194 directed step using CRISPR-Cas9.
195
196 **One-step generation of rapamycin resistant CAR-T cells**
197 To improve targeting efficacy, we delivered the CD19-CAR-2A-EGFP donor using an adeno-
198 associated virus 6 (AAV6) vector[10,11,20] (**Fig. 3a**). Following Cas9 RNP nucleofection, $CD3^+$ T
199 cells isolated from whole blood (Donor ID: WB 1) were transduced with the AAV6 vector in a
200 small volume for 8 hours and then transferred to the culture medium for three days before
201 rapamycin treatment. Cells were reactivated four days post-transfection and expanded for an
202 additional 7 days before quantification of transgene-expressing cells (**Fig. 3b**). We observed a
203 substantial increase in editing efficacy both pre and post 8 days of selection as determined by out-
204 out PCR and Sanger sequencing in the bulk populations (**Fig. 3c**). Yields of CAR-2A-$EGFP^+$ cells
205 reached 82% and 85% at MOIs of $5x10^3$ and $1x10^4$, respectively as determined by FACS-based
206 analysis (**Fig. 3d**). These results were reproduced with $CD3^+$ T cells isolated from a second whole
207 blood donor (Donor ID: WB2) and two LRS donors (Donor ID: LRS1, LRS2) (**Fig. 3e**). In total,
208 cells from four distinct healthy donors generated similar outcomes, albeit with lower efficiency
209 when using cells isolated from LRS chambers (**Fig. 3e**).
210
211 To test for functionality, we performed luciferase-based cytotoxicity assays with selected CAR-T
212 effector cells and $CD19^+$ NALM6 target cells stably expressing firefly luciferase and RFP. We
213 also generated a rapamycin-resistant NALM6 cell line (NALM6-RapaR) by installing the *MTOR*-
214 F2108L mutation to assess the combinational impact of rapamycin. We observed high levels of
215 cytotoxicity with and without rapamycin at the highest effector to target ratios (**Fig. 3f**). At lower
216 effector to target ratios, higher levels of cytotoxicity were observed in the presence of rapamycin,
217 confirming that these CAR-T cells can be used in combination with the mTOR inhibitor to target

218 cancer cells (**Fig. 3f**). This combinatorial effect was not observed with NALM6-RapaR cells (**Fig.**
219 **3f**). These data indicate that immunosuppressive doses of rapamycin can be used in combination
220 with these CAR-T cells to increase antitumor activity *in vitro*.
221
222 Rapamycin has previously been shown to accelerate the memory T-cell differentiation program
223 and may impact the phenotype of treated cells[48,49]. To begin to probe the impact of rapamycin
224 treatment *ex vivo*, we analyzed differentiation and exhaustion markers and performed multi-color
225 flow cytometry panels after 8 and 15 days of treatment using $CD3^+$ T cells isolated from whole
226 blood of two additional healthy donors (ID: WB3, WB4) (**Supplementary Fig. 7**). In these
227 experiments, editing rates remained high (~80% CAR-2A-$EGFP^+$ cells) and we observed a
228 minimal impact of rapamycin treatment on the expression of differentiation and exhaustion
229 markers, as determined by CD4, CD8, CD45RO, CCR7, and PD1 staining, on both rapamycin-
230 sensitive and rapamycin-resistant T cells (**Supplementary Fig. 7**). Rapamycin-resistant CAR-2A-
231 $EGFP^+$ populations displayed a mix of central memory ($CCR7^+/CD45RO^+$) and effector memory
232 ($CCR7^-/CD45RO^+$) T cells after 8 days of treatment with rapamycin, while most cells displayed
233 an effector memory ($CCR7^-/CD45RO^+$) phenotype after 15 days of treatment (**Supplementary**
234 **Fig. 7**). Overall, rapamycin treatment (25 nM) had little impact on T cells' differentiation in our
235 *ex vivo* expansion protocol, and our 14 days expansion timeline (8 days of rapamycin treatment)
236 yields a mix of central memory and effector memory CAR-T cells.
237
238 **Combinatorial CAR-T cell therapy with rapamycin slows leukemia progression *in vivo***
239 We then established a xenograft leukemia model using NOD/SCID/IL-2Rγ-null (NSG) male and
240 female mice injected with NALM6 cells stably expressing RFP and firefly luciferase. NALM6
241 cells were injected intravenously, and rapamycin treatment (4 mg/kg, daily) started three days
242 later. Rapamycin-resistant CD19-CAR-2A-$EGFP^+$-CAR T cells (Donor ID: WB2, see **Fig. 3e**),
243 which underwent *ex vivo* selection with 25 nM rapamycin for eight days (see **Fig. 3a,b)** , were
244 administered intravenously four days after tumor inoculation (**Fig. 4a)**. In total, these CD19-CAR
245 T cells where expanded *ex vivo* for 14 days and stimulated twice before being injected in mice (see
246 **Fig. 3b)**. As a negative control, we used $CD3^+$ T cells untransduced (UT) with AAV6 donors but
247 having undergone nucleofection with the Cas9-*MTOR*-G4 RNP. Tumor engraftment and
248 progression were assessed via bioluminescence imaging twice per week for seven weeks. While

249 rapid tumor progression was observed with UT T cells without treatment, rapamycin slowed tumor
250 progression and conferred an additional week of survival (**Fig. 4b,c)**. Of importance, rapamycin-
251 resistant CD19-CAR-T cells selected *ex vivo* could efficiently target NALM6 cells *in vivo* in the
252 presence or absence of rapamycin (**Fig. 4b,c)**. Combinatorial rapamycin administration with
253 rapamycin-resistant CAR-T cells further slowed tumor progression and allowed the mice to
254 survive for up to seven weeks post-tumor inoculation (**Fig. 4b,c)**. While we observed antitumor
255 control during the first weeks, tumors eventually rebounded and killed all mice (**Fig. 4b,c)**. Our
256 results corroborate previous findings demonstrating the limited persistence of second-generation
257 CARs harboring a CD28 costimulation domain compared to 4-1BB[50–52]. Indeed, the second-
258 generation CD19-CAR architecture used during this study[53] contains a CD28 transmembrane
259 domain, which can form an heterodimer with CD28[54], and a CD28 costimulation domain that has
260 been linked to lower persistence compared to 4-1BB[6,52,55]. Nevertheless, our results confirmed that
261 our targeting strategy can create functional rapamycin-resistant CAR-T cells that can be used in
262 combination with rapamycin to slow tumor progression *in vivo*, offering an opportunity to target
263 cancer cells' metabolism to facilitate tumor eradication.
264
265 **Pharmacological control of CAR-T cell activity using rapamycin**
266 Using intracellular[56] or extracellular[46] rapamycin-regulated dimerization domains to
267 pharmacologically control chimeric antigen receptor assembly is a promising approach for
268 developing safer CAR-T cell therapies[57]. However, these systems rely on the non-
269 immunosuppressive rapamycin analog AP21967 which was primarily developed as a tool for
270 chemical biology and do not have suitable pharmacokinetic properties for clinical use[56], or on non-
271 immunosuppressive doses of rapamycin, which limit their clinical potential. Thus, we tested
272 whether we could target a dimerizing agent-regulated immunoreceptor complex (DARIC)[46], which
273 can be toggled between on and off states using rapamycin, to the *MTOR* locus.
274
275 Building on previous studies[10,46], we sought to test whether multiplexed targeting of separate
276 DARIC components could be performed at the *MTOR* and *TRAC* loci simultaneously (**Fig. 5a**).
277 Taking advantage of the dynamic regulation of CAR expression at the *TRAC* locus[10], which averts
278 tonic CAR signaling, we targeted a CD22 recognition domain (DARIC 2) and a 41BB-CD3z
279 signaling domain (DARIC 3) linked by a P2A self-cleaving peptide to the *TRAC* locus (**Fig. 5a**).

280 In parallel, we targeted an additional CD19 recognition domain (DARIC 1) to the *MTOR* locus to
281 confer dominant cellular resistance to rapamycin while providing an additional antigen specificity
282 to potentially overcome antigen escape[6,7,55,58,59]. Multiplexed targeted integration of both DARIC
283 cassettes was observed at *MTOR* and *TRAC*, as determined by out-out PCR (**Fig. 5b**). An average
284 of 58% of alleles harboring the *MTOR*-F2108L was observed, confirming that multiplexed genome
285 editing did not decrease targeted transgene integration at *MTOR* (**Fig. 5b**). We performed FACS-
286 based cytotoxicity assays using unselected CAR-T cells in the presence or absence of 25 nM
287 rapamycin with DARIC-T cells that were resistant (RapaR-CD19-CD22-DARIC) or not (CD22-
288 DARIC) to rapamycin. Strikingly, cytotoxicity was only observed with rapamycin-resistant CD19-
289 CD22-DARIC-T cells in the presence of rapamycin, confirming DARIC immunoreceptor
290 dimerization only in the presence of the drug (**Fig. 5c**). As observed above, rapamycin inhibited
291 NALM6 cell growth to some extent, but not NALM6-RapaR which harbors the *MTOR*-F2108L
292 mutation (**Fig. 5c**). Rapamycin-sensitive CD22-DARIC-T cells, where the *MTOR*-F2108L-
293 DARIC-1 AAV6 donor was omitted during transduction, could not target cancer cells in the
294 presence of an immunosuppressive dose of 25 nM rapamycin (**Fig. 5c**). We note that the CD22
295 scFv construction (DARIC 2) we engineered has never been tested for functionality by itself, thus
296 the absence of cytotoxicity of CD22-DARIC cells in presence of rapamycin should be interpreted
297 with caution. Altogether, this multiplexed strategy offers the opportunity to use
298 immunosuppressive doses of rapamycin in combination with DARIC-T cells to decrease tumor
299 cell growth and to pharmacologically fine-tune CAR-T cells' activity.
300

301 **DISCUSSION**

302 Engineering primary T cells with programmable nucleases for cell therapy applications remains
303 challenging. In this work, we describe a marker-free selection approach to simultaneously target a
304 therapeutic transgene of interest and a point mutation to the *MTOR* locus to generate dominant
305 cellular resistance to rapamycin. We show that mTORC1 signaling remained functional and cells
306 grew robustly in the presence of rapamycin after targeted transgene integration. Our results further
307 demonstrate that introns provide an additional non-coding location for targeted transgene
308 integration via intron nesting[32,33]. Taking advantage of this naturally occurring genomic
309 architecture allows the co-modification of an endogenous gene during the integration of a
310 therapeutic transgene of interest in a single gene editing event. However, this strategy is limited to

311 moderately active promoters, such as the human *PGK1* promoter used in this study, since
312 transcriptional interference between the overlapping genes[33] would be detrimental for mTORC1
313 signaling, and consequently, CAR-T cell activation and expansion[21,30]. This could be prohibitive
314 for applications where high levels of transgene expression are needed to reach a therapeutic
315 threshold.
316
317 The metabolic competition between cancer and T cells has previously been shown to drive cancer
318 progression[60], and metabolic interventions could be used in combination to improve clinical
319 outcomes[61]. Hence, targeting cancer metabolism via mTORC1 inhibition could potentially slow
320 tumor progression and facilitate complete tumor eradication. Taken together, our findings suggest
321 that rapamycin could be administered to enrich CRISPR-engineered cells *in vivo* while providing
322 a fitness advantage against tumor cells. Of note, since double editing events at two different loci
323 are not statistically independent, rapamycin co-selection could also be performed to enrich a
324 second modification of interest[32,62].
325
326 Our cytotoxicity assays corroborate previous findings regarding the combinatorial impact of
327 rapamycin with *piggyBac*-modified rapamycin-resistant CAR-T cells[27]. Nonetheless, our
328 CRISPR-based strategy offers advantages over the use of a two *piggyBac* transposon vectors
329 system to target a CAR and a large rapamycin-resistant mTOR transgene cassette (≈7.65kb)[27] to
330 random genomic locations[27–29].
331
332 While we focused on the standard CD19^{+} NALM6 acute lymphoblastic leukemia model during
333 this study, combinatorial CAR-T cell therapy with rapamycin could potentially improve antitumor
334 activity against solid tumors displaying hyperactive mTOR signaling[34,63,64]. Moreover, using a
335 dimerizing agent-regulated immunoreceptor complex (DARIC) switchable between on and off
336 states using rapamycin is a promising strategy to develop safer CAR-T cells therapies[46,57]. One
337 limitation of this system is the use of non-immunosuppressive rapamycin dosing[46] to prevent the
338 inhibition of CAR-T cells' activation, which could be overcome using rapamycin-resistant
339 DARIC-T cells. This system could be used to fine-tune CAR-T cells activity with rapamycin
340 pulsing to prevent tonic CAR signaling, and consequently, exhaustion[46,65]. In line with this,
341 transient rest induced by a drug-regulatable CAR or the tyrosine kinase inhibitor dasatinib has

342 been shown to restore functionality in exhausted CAR-T cells through epigenetic remodeling[66–68].
343 Most importantly, rapamycin-regulatable CAR architectures could be used as safety switches to
344 dampen toxicity and severe adverse events associated with cytokine release syndrome[46,66–70].
345
346 During this study, we also identified new rapamycin resistance mutations via saturation prime
347 editing that displayed intermediate levels of mTORC1 signaling in the presence of rapamycin.
348 These additional mutations offer interesting opportunities to investigate the potential of
349 pharmacologically fine-tuning mTORC1 activity for cell therapy applications. mTOR plays key
350 in T cell fate decisions and differentiation[30,48]. Reducing mTORC1 signaling has been shown to
351 trigger the formation of stem cell-like memory T cells and also enhance CAR-T cell antitumor
352 activity[49,71]. In addition, Lamarthée and colleagues have shown that transient mTOR inhibition
353 with rapamycin rescues 4-1BB CAR-Tregs from tonic signal-induced dysfunction[72]. Considering
354 that mTORC1 signaling acts as a metabolic rheostat[24], fine-tuning this pathway could potentially
355 have a positive impact on CAR-T cells persistence, and consequently, CAR-T cells antitumor
356 activity. While this hypothesis warrants further investigation, our results demonstrate that
357 engineering the *MTOR* locus with CRISPR allows the marker-free selection of cells with different
358 levels of mTORC1 signaling in the presence of rapamycin.
359
360 Altogether, the strategy presented here should facilitate the *ex vivo* and *in vivo* enrichment of
361 CRISPR-engineered cells expressing a therapeutic transgene of interest, providing a versatile
362 platform for cell therapy applications.
363

364 # METHODS

365 **K562 and NALM6 cell culture and transfection**

366 K562 cells were obtained from the ATCC (CCL-243) and NALM6 cells stably transduced to
367 express a FLUC-T2A-RFP-IRES-Puro reporter gene cassette (Biosettia) were gently provided by
368 Scott McComb (National Research Council of Canada). K562 and NALM6 cells were maintained
369 at 37 °C under 5% CO_2 in RPMI medium supplemented with 10% FBS, penicillin–streptomycin,
370 and GlutaMAX. Cells were routinely tested for the absence of mycoplasma contamination.
371 Rapamycin (Cayman Chemicals, Cat 53123-88-9) was dissolved at 10 mg/ml in DMSO, working
372 dilutions were prepared in water and stored at -20ºC. AZD8055 (STEMCELL Technologies) was

373 dissolved at 10 mM in DMSO, working dilutions were prepared in water and stored at -20ºC.
374 DMSO alone was diluted in water and used as vehicle control. Ouabain octahydrate (Sigma) was
375 dissolved at 5 mg/ml in hot water, working dilutions were prepared in water and stored at -20ºC.
376 K562 and NALM6 cells ($2x10^5$ cells/transfection) were transfected using a Lonza 4D
377 nucleofector™ with a SF nucleofection kit (Lonza) following manufacturer's recommendations.
378 For prime editing transfections, K562 cells were transfected with 0.75 µg of PE vector, 0.25 µg of
379 epegRNA vector, and 0.1 µg of nick sgRNA vector. NALM6 cells were transfected with 50 pmols
380 of SpCas9 RNP (IDT) and 0.75 µg of dsDNA donor harboring *MTOR*-F2108L and a PAM
381 mutation to generate the NALM6-RapaR cell line. Cells were treated with the indicated
382 concentration of rapamycin 3 days post-nucleofection until all non-resistant cells were eliminated.
383

384 **Genome editing vectors and recombinant AAV production**

385 Guide RNAs were designed with CRISPOR[41] and their sequences are provided in the
386 **Supplementary material** section. When required, DNA sequences for the guides were modified
387 at position 1 to encode a G, owing to the transcription requirement of the human U6 promoter.
388 Guide RNAs were cloned into pX330-U6-Chimeric_BB-CBh-hSpCas9 (a gift from Feng Zhang;
389 Addgene 42230) and their sequences are provided in the **Supplementary material** section.
390 Plasmid donors were cloned into pUC19 with short homology arms (700-800 bp) and all sequences
391 were confirmed by Sanger sequencing. Prime editing (PE) experiments were performed with
392 pCMV-PEmax[73] (a gift from David Liu; Addgene 174820), and pU6-tevopreq1-GG-acceptor[39] (a
393 gift from David Liu; Addgene 174038). To repurpose the mTORC1 signaling reporter mVenus-
394 TOSI previously developed for mouse[38], the N-terminal residues (1-82) of the human *PDCD4*
395 gene were codon optimized using the GenSmart™ codon optimization tool, synthesized as a
396 gBlocks™, and cloned into ATP1A1_T804N_hPGK1_mScarlet-I_Donor (Addgene 173207)
397 upstream of the mScarlet-I-NLS cassette using AflII and NcoI. The CD19-CAR-28z-2A-EGFP
398 gene cassette from pSLCAR-CD19-28z (a gift from Scott McComb: Addgene 135991)[53] was
399 cloned into the *MTOR* donor vector by Gibson assembly without the 3xFLAG. The CD19-DARIC
400 expression vector was designed in-house based on previously described constructions[46] and US
401 patent 2012/0266971 A1. The CD22-DARIC construction was designed using a previously
402 described CD22 scFv fragment[59]. DARIC sequences were codon-optimized using GenSmart™
403 codon optimization tool, synthesized by GenScript, and cloned into the AAV6 vector using Gibson

404 assembly. Donor sequences are provided in the **Supplementary material** section. The AAV6
405 vectors were produced by the vector core facility at the Canadian neurophotonics platform
406 (molecular tools). ITR integrity was assessed following BssHII digestion of the AAV plasmid
407 before production. The virus was resuspended in PBS 320 mM NaCl + 5% D-sorbitol + 0.001%
408 pluronic acid (F-68), aliquoted, and stored at −80°C. The vector yields were $1x10^{12}$, $8.5x10^{12}$, and
409 $6.9x10^{12}$ GC/ml for the *MTOR*-F2108L-CD19-CAR-2A-EGFP, *MTOR*-F2108L_CD19_scFv, and
410 TRAC_T2A_CD22-DARIC donors, respectively.
411
412 **Primary human T cells isolation and culture**
413 Primary $CD3^+$ human T cells were isolated from anonymized healthy human donors either from
414 fresh whole blood (WB) or leukocyte reduction system (LRS) chambers (Héma-Québec), or from
415 human peripheral blood leukopaks (STEMCELL). EasySep™ Human T cell isolation kit
416 (STEMCELL) or CD3 microbeads (Miltenyi) were used for positive magnetic selection of $CD3^+$
417 T cells from peripheral blood mononuclear cells (PBMCs). Primary $CD3^+$ T cells were cultured
418 with Immunocult-XF T cell expansion medium supplemented with 1% penicillin-streptomycin and
419 300 U/ml IL-2. Cells were thawed and activated for 3 days with Immunocult™ human
420 CD3/CD28/CD2 T cell activator (STEMCELL) before nucleofection.
421
422 **Primary human T cells transfection**
423 dsDNA donors were produced as described previously[45]. Briefly, donor sequences were cloned
424 into a cloning vector and PCR amplification (25 cycles) was performed using Kapa-HiFi
425 polymerase (Roche). DNA purification was performed by solid-phase reversible immobilization
426 using AMPure XP (Beckman Coulter) magnetic beads. For ribonucleoprotein complex (RNP)
427 formulation, 100 pmols of sgRNAs (Alt-R, IDT) were mixed with 0.8 µl of 100 mg/ml
428 polyglutamic acid (Sigma) and 50 pmols of SpCas9 nuclease (IDT) as previously described[74]. The
429 RNP mix was incubated at 37°C for 10 minutes and the dsDNA donors were added to the mix and
430 incubated at room temperature for 5 minutes before transfection. Primary $CD3^+$ T cells ($1x10^6$
431 cells/transfection) were transfected using a Lonza 4D nucleofector™ (Pulse code EH115) with a
432 P3 nucleofection kit (Lonza) following manufacturer's recommendations with the indicated DNA
433 concentrations. $CD3^+$ T cells were resuspended in 80 µl media without IL-2 directly after
434 nucleofection and incubated at 37°C for 15 minutes before transfer into culture media plates at

435 $1x10^6$ cells/ml. For AAV6 transduction, $CD3^+$ T cells were resuspended in 80 µl media directly
436 after nucleofection and AAV6 vectors were added. Cells were incubated at 37ºC for 8 hours at
437 high cell density before transfer into culture media plates. For rapamycin selection, $CD3^+$ T cells
438 were treated with or without 25 nM rapamycin on Day 3 post-nucleofection, restimulated with
439 Immunocult™ human CD3/CD28/CD2 T cell activator (STEMCELL) 4 days post-transfection,
440 and expanded for an additional 7 days.
441
442 **Sanger sequencing analysis and out-out PCRs**
443 Genomic DNA was extracted with QuickExtract DNA extraction solution (EpiCentre) following
444 manufacturer's recommendations. Primers used in this study and the PCR product sizes are
445 provided in the **Supplementary material** section. PCR amplifications were performed with 30
446 cycles of amplification with Phusion polymerase. Sanger sequencing was performed on PCR
447 amplicons to quantify the percentage of edited alleles using TIDE[75], TIDER[76], and BEAT[77]. To
448 quantify the percentage of alleles harboring the *MTOR*-F2108L mutation after targeted transgene
449 integration, we performed PCR amplifications to amplify both WT and HDR alleles with a forward
450 primer binding outside the region of homology of our donors, and a reverse primer binding inside
451 the homology arm upstream of the SpCas9 target sites (out-in PCR). Genomic DNA from WT
452 cells and cells transfected or transduced only with the donor were used as negative controls in all
453 experiments. Kapa-HiFi polymerase was used for out-out PCRs. To detect targeted integration,
454 out-out PCRs were performed with primers that bind outside of the homology regions of the
455 plasmid/dsDNA donors. Wild type K562 or $CD3^+$ T cells genomic DNA was used as a control for
456 all PCRs.
457
458 **Flow cytometry**
459 The percentage of fluorescent cells was quantified using a BD LSRII flow cytometer using
460 FACSdiva v6.1.2 software, and $1x10^5$ cells were analyzed for each condition. For mTORC1
461 signaling assays, cells were washed with PBS and cultured at least 3 days without rapamycin. Cells
462 were treated with the indicated concentration of rapamycin or AZD8055 for 24 hours before
463 analysis. FACS sorting was performed using a BD FACS Aria Fusion flow cytometer for the
464 saturation prime editing experiment, and $5x10^5$ cells were sorted for each condition.
465

466 Multicolor flow cytometry panels were performed using a Cytek Aurora flow cytometer. T cells
467 were stained with fixable viability dye eF506 (Invitrogen Cat 65-0866-18) for 15 minutes at 4ºC,
468 then washed and resuspended in Human TruStain FcX blocking solution (BioLegend Cat
469 2711505) and Brilliant Stain Buffer Plus (BD Biosciences Cat 566385) for 10 minutes at room
470 temperature. After blocking, cells were stained with the following antibody cocktail diluted in flow
471 cytometry staining buffer: mouse anti-human CD3 BV750 (BioLegend Cat 344846), mouse anti-
472 human CD4 AF700 (BioLegend Cat 300526), mouse anti-human CD8 PerCP (BioLegend Cat
473 301030), mouse anti-human CD279 BV421 (BioLegend Cat 329920), mouse anti-human CCR7
474 APC-Fire 750 (BioLegend Cat 353246), and mouse anti-human CD45RO PE-Cy7 (Invitrogen Cat
475 25-0457-42). Flow cytometric data were analyzed using SpectroFlo (Cytek) and FlowJo V10 (Tree
476 Star).
477
478 **Saturation prime editing and high-throughput DNA sequencing**
479 The *MTOR*-F2108 saturation epegRNA (tevopreQ1)[39] vector was designed to install NNK codons
480 and a silent R2109R PAM mutation at *MTOR* exon 45, synthesized as a gBlock™ (IDT), and
481 cloned into pU6-tevopreq1-GG-acceptor[39] (a gift from David Liu; Addgene 174038). K562 cells
482 stably expressing the mSc-TOSI reporter were transfected with PE3max-epegRNA (tevopreQ1)
483 vectors and treated with 0.5 μM rapamycin starting 3 days post-transfection until all non-resistant
484 cells were eliminated. Following selection, cells were treated for 24 hours with 0.5 μM rapamycin
485 and FACS-sorted for low mSc-TOSI fluorescence intensity to enrich cells with functional
486 mTORC1 signaling in the presence of rapamycin. Genomic DNA was harvested after selection
487 and after FACS sorting for low and high mSc-TOSI fluorescence intensity. For amplicons
488 sequencing, primers containing Illumina forward and reverse adapters were used for a first round
489 of PCR using the Kapa-HiFi polymerase. PCR products were purified using AMPure XP magnetic
490 beads and their quality was evaluated by electrophoresis. A second round of PCR and bead
491 purification was performed for indexing, and amplicons were sequenced on an Illumina MiSeq
492 instrument. Alignment of amplicon sequences to the reference *MTOR* sequence was performed
493 using CRISPResso2[78], and all possible NNK codons were detected.
494
495 **GUIDE-Seq**

496 GUIDE-Seq was performed as previously described[43,44], except for improvements of the Next
497 Generation Sequencing (NGS) library preparation procedure reported below. GUIDE-Seq oligos
498 harboring 5' phosphorylation modification and two phosphorothioate linkages between the last
499 two nucleotides at the 3' end were synthesized by IDT. Oligos were mixed in 50 mM NaCl, 10
500 mM Tris-HCl (pH 8.0), 1 mM EDTA, and annealed by heating the solution to 95°C for 10 minutes,
501 followed by gradual cooling on a thermocycler. For K562 cells, $2x10^5$ cells were electroporated
502 with 750 ng of SpCas9-sgRNA vectors and 100 pmol of annealed GUIDE-Seq oligos. For primary
503 $CD3^+$ T cells, $1x10^6$ cells were electroporated with 50 pmol SpCas9 RNP and 100 pmol annealed
504 GUIDE-Seq oligos. Genomic DNA was harvested using QIAmp UCP DNA Micro Kit (QIAGEN).
505 GUIDE-Seq oligo tag integration was confirmed using TIDE[75] and DECODR[79] webtools from
506 Sanger sequencing. The library preparation method was improved starting from the original
507 GUIDE-Seq procedure[43,44]. After mechanical fragmentation, end-repair and A-Tailing were
508 directly performed using the NEBNext UltraII DNA kit (New England Biolabs). A new custom
509 universal Y-adapter based on the Illumina TruSeq sequences was designed to include a Unique
510 Molecular Index (UMI) in the sequencing read instead of the index read. This modification enables
511 mixing of GUIDE-Seq libraries with other Illumina library types (amplicon, shotgun, RNASeq,
512 etc.) in the sequencing run by using standard index read lengths. This new adapter was ligated as
513 described in the instructions of the NEBNext UltraII procedure using a final concentration of 133
514 nM. Ligated DNA was purified using 0.9X volume of AMPure XP beads (Beckman-Coulter), then
515 split in 2 for PCR amplifications with either Minus or Plus primers using Q5 DNA Polymerase
516 (New England Biolabs) with the following cycling conditions: 98°C 30 sec; 10 cycles of 98°C 10
517 sec, 55°C 30 sec, 72°C 30 sec; 15 cycles of 98°C 10 sec, 65°C 30 sec, 72°C 30 sec; 72°C 2 min;
518 4°C hold. New primers with Illumina sequence tails were specifically designed for this improved
519 method. The use of Illumina sequences at the Plus/Minus amplification stage eliminates the use of
520 custom primers for sequencing. PCR products were purified with 0.9X AMPure XP beads and
521 quantified using Qubit dsDNA HS Assay (Invitrogen). Then, 10 ng DNA was used for a second
522 PCR amplification with Illumina TruSeq dual-indexing primers (98°C 30 sec; 8 cycles of 98°C 10
523 sec, 55°C 30 sec, 72°C 30 sec; 72°C 2 min; 4°C hold). The barcoding at the PCR stage enables a
524 much simpler and higher multiplexing capacity. PCR products were purified using 0.85X AMPure
525 XP beads, quantified using Qubit dsDNA HS Assay and ran on a Bioanalyzer High Sensitivity
526 DNA chip (Agilent). Samples were pooled in equimolar amounts and sequenced on 1.4% (35M

527 read block) of a NovaSeq S4 PE150 lane (Illumina) at the Centre d'Expertise et de Services
528 Génome Québec (Montréal, QC). The remaining portion of the sequencing lane contained a
529 mixture of library types from multiple organisms (*M. plutonius*, *P. larvae*, *F. graminearum*, *P.*
530 *neglectus*, *Colletotrichum* spp., *Sporothrix* spp.).
531
532 **Analysis of GUIDE-Seq sequencing**
533 A new pipeline, named guideseq_ibis, was designed to analyze the data from the improved
534 GUIDE-Seq procedure (https://github.com/enormandeau/guideseq_ibis). Using this pipeline, the
535 raw reads were trimmed for quality using trimmomatic (v0.36, min_length 100, crop_length 200).
536 Then, only reads containing the expected alien sequence (maximum hamming distance of 1) and
537 only one copy of the ODN sequence (maximum hamming distance of 6) were retained. For these
538 reads, the Unique Read Identifiers (UMIs) and first eight nucleotides were used to rename the
539 sequence. These tagged reads were then mapped onto the latest GRCh38 human genome assembly
540 with bwa (v0.7.17-r1188, -T 10) and then samtools (v1.12, -S -q 1 -F 4 -F 256 -F 2048). The
541 alignment sam files were then sorted by chromosome name and position. The UMI and eight first
542 nucleotides of the reads and the starting positions of their alignments were used to detect duplicated
543 reads. Namely, only one copy of reads with identical UMIs, eight first nucleotides, and alignment
544 start position were kept. Then, Double Stranded Breaks (DSBs) were identified. For this, alignment
545 sites were scanned for peaks of coverage in decreasing order of depth of coverage and pairs of
546 ODN+ and ODN- were reported until the pairs did not meet the minimum coverage threshold
547 (min_length 100, min_coverage 50, window_size 10, position_error 5, bin_size 10000). To
548 account for small errors in sequencing and mapping, read counts are collected within
549 `window_size` nucleotides around each peak and pairs of ODN sequences were kept if they fell
550 withing `position_error` nucleotides of their relative expected positions. Identified sequences on
551 target and off-target were reported for each sample with their chromosome and position
552 localisation, the identifier and name of any gene they overlapped (using a simplifited annotation
553 table from GRCh38.p14), and metrics about the counts of the ODN+ and ODN- reads. Finally,
554 annotation of the found targets and off-targets was performed to add information about the guide's
555 name, the distance between the target sequence and the expected guide sequence, as well as a
556 representation of the modified nucleotides along the guide sequence.
557

558 **Cytotoxicity assays**

559 Luciferase-based cytotoxic assays were performed as previously described[10,80]. After rapamycin
560 selection, CD19-CAR-T cells were washed with PBS, and co-cultured in 96-well plates in
561 supplemented RPMI medium with NALM6 cells stably expressing firefly luciferase and RFP at
562 the indicated effector to target ratio (E:T) for 18 hours. Target cells incubated with WT $CD3^+$ T
563 cells were used to determine maximal luciferase expression (maximal relative light units; RLU_{max}).
564 After coculture, an equal volume of luciferase substrate (Bright-Glo, Promega) was added to each
565 well. Emitted light was detected with a Tecan luminescence plate reader and cell lysis was
566 determined as $(1 – (RLU_{sample})/(RLU_{max})) \times 100$. FACS-based cytotoxicity assays were performed
567 as previously described[46], except with a prolonged coculture time. T cells were washed with PBS,
568 and cocultured in 12-well plates in supplemented RPMI medium with 50:50 mixtures of
569 rapamycin-resistant K562-EBFP (CD19-negative) cells and NALM6-RFP cells at the indicated
570 effector to target ratio (E:T) for 72 hours. Cell viability was assessed using the fixable viability
571 dye eFluor™ 660 (eBioscience). The ratio of viable NALM6-RFP and K562-EBFP cells following
572 coculture in the presence or absence of 25 nM rapamycin was used to calculate the percentage of
573 cytotoxicity. Target cells incubated with WT $CD3^+$ T cells were used to determine maximal
574 NALM6-RFP growth.

575

576 **Mouse systemic tumor model.**

577 The *in vivo* CAR-T cells experiments were performed according to the *Canadian Guide for the*
578 *Care and Use of Laboratory Animals*. The Université Laval Animal Care and Use Committee
579 approved the procedure. 8-10 weeks-old NOD/SCID/IL-2Rγ-null (NSG) male and female mice
580 were acquired from Jackson Laboratory. 0.5×10^6 NALM6-RFP-FLUC cells were administered
581 via tail vein injection. Three days later, daily rapamycin treatment (4 mg/kg) or vehicle (filter-
582 sterilized solution of 5% Tween80, 5% PEG-400, 0.7% DMSO) was administered by
583 intraperitoneal (IP) injection. Four days after tumor inoculation, 2×10^6 CAR-T cells (≈86% CAR-
584 2A-$EGFP^+$ cells) or untransduced (UT) T cells were administered via tail vein injection. CAR-T
585 cells expanded for 14 days, including 8 days of treatment/selection with 25 nM rapamycin, were
586 used for the *in vivo* experiment. Tumor burden was measured twice per week by bioluminescence
587 imaging using the IVIS LuminaIII Imaging System (PerkinElmer). Mice were anesthetized using
588 isoflurane, and 150 mg/kg D-Luciferin (Goldbio) was administered via IP injection. Data were

589 analyzed using the Living Image software (PerkinElmer). The maximum tumor burden and
590 survival endpoint were defined by hindlimb paralysis or other clinical signs of distress. There were
591 no instances in which this maximum tumor burden was exceeded.
592

593 **DATA AVAILABILITY**

594 Source data for the figures are provided as a Source Data file. All raw Sanger sequencing data
595 generated in this study are available on request from the corresponding author [YD].
596

597 **CODE AVAILABILITY**

598 The adapted GUIDE-Seq analysis pipeline developed and used in this study is freely available at
599 https://github.com/enormandeau/guideseq_ibis.
600

601 **REFERENCES**

602 1. Brentjens, R. J. *et al.* CD19-targeted t cells rapidly induce molecular remissions in adults
603 with chemotherapy refractory acute leukemia. *Sci. Transl. Med.* **5**, 177ra38 (2013).
604 2. Lee, D. W. *et al.* T cells expressing CD19 chimeric antigen receptors for acute
605 lymphoblastic leukaemia in children and young adults: A phase 1 dose-escalation trial.
606 *Lancet* **385**, 517–528 (2015).
607 3. Neelapu, S. S. *et al.* Axicabtagene ciloleucel CAR T-cell therapy in refractory large B-
608 Cell lymphoma. *N. Engl. J. Med.* **377**, 2531–2544 (2017).
609 4. Park, J. H. *et al.* Long-term follow-up of CD19 CAR therapy in acute lymphoblastic
610 leukemia. *N. Engl. J. Med.* **378**, 449–459 (2018).
611 5. Maloney, D. G. Anti-CD19 CAR T cell therapy for lymphoma — off to the races! *Nat.*
612 *Rev. Clin. Oncol.* **16**, 279–280 (2019).
613 6. Labanieh, L., Majzner, R. G. & Mackall, C. L. Programming CAR-T cells to kill cancer.
614 *Nat. Biomed. Eng.* **2**, 377–391 (2018).
615 7. Larson, R. C. & Maus, M. V. Recent advances and discoveries in the mechanisms and
616 functions of CAR T cells. *Nat. Rev. Cancer* **21**, 145–161 (2021).
617 8. Bailey, S. R. & Maus, M. V. Gene editing for immune cell therapies. *Nat. Biotechnol.* **37**,
618 1425–1434 (2019).
619 9. Ellis, G. I., Sheppard, N. C. & Riley, J. L. Genetic engineering of T cells for

620 immunotherapy. *Nat. Rev. Genet.* **16**, 103–107 (2021).
621 10. Eyquem, J. *et al.* Targeting a CAR to the TRAC locus with CRISPR/Cas9 enhances
622 tumour rejection. *Nature* **543**, 113–117 (2017).
623 11. Mansilla-soto, J. *et al.* HLA-independent T cell receptors for targeting tumors with low
624 antigen density. *Nat. Med.* **28**, 345–352 (2022).
625 12. Wei, J. *et al.* Targeting REGNASE-1 programs long-lived effector T cells for cancer
626 therapy. *Nature* **576**, 471–476 (2019).
627 13. Giuffrida, L. *et al.* CRISPR/Cas9 mediated deletion of the adenosine A2A receptor
628 enhances CAR T cell efficacy. *Nat. Commun.* **12**, 3236 (2021).
629 14. Carnevale, J. *et al.* RASA2 ablation in T cells boosts antigen sensitivity and long-term
630 function. *Nature* **609**, 174–182 (2022).
631 15. Depil, S., Duchateau, P., Grupp, S. A., Mufti, G. & Poirot, L. 'Off-the-shelf' allogeneic
632 CAR T cells: development and challenges. *Nat. Rev. Drug Discov.* **19**, 185–199 (2020).
633 16. Stadtmauer, E. A. *et al.* CRISPR-engineered T cells in patients with refractory cancer.
634 *Science* **7365**, eaba7365 (2020).
635 17. Ottaviano, G. *et al.* Phase 1 clinical trial of CRISPR-engineered CAR19 universal T cells
636 for treatment of children with refractory B cell leukemia. *Sci. Transl. Med.* **3010**,
637 eabq3010 (2022).
638 18. Shy, B. R. *et al.* High-yield genome engineering in primary cells using a hybrid ssDNA
639 repair template and small-molecule cocktails. *Nat. Biotechnol.* (2022)
640 doi:10.1038/s41587-022-01418-8.
641 19. Paul, B. *et al.* Efficient enrichment of gene-modified primary T cells via CCR5-Targeted
642 integration of mutant dihydrofolate reductase. *Mol. Ther. Methods Clin. Dev.* **9**, 347–357
643 (2018).
644 20. Wiebking, V. *et al.* Metabolic engineering generates a transgene-free safety for cell
645 therapy. *Nat. Biotechnol.* **38**, 1441–1450 (2020).
646 21. Saxton, R. A. & Sabatini, D. M. mTOR signaling in growth, metabolism, and disease. *Cell*
647 **168**, 960–976 (2017).
648 22. Battaglioni, S., Benjamin, D., Wälchli, M., Maier, T. & Hall, M. N. mTOR substrate
649 phosphorylation in growth control. *Cell* **185**, 1814–1836 (2022).
650 23. Liu, G. Y. & Sabatini, D. M. mTOR at the nexus of nutrition, growth, ageing and disease.

651 *Nat. Rev. Mol. Cell Biol.* **21**, 183–203 (2020).
652 24. Valvezan, A. J. & Manning, B. D. Molecular logic of mTORC1 signalling as a metabolic
653 rheostat. *Nat. Metab.* **1**, 321–333 (2019).
654 25. Mossmann, D., Park, S. & Hall, M. N. mTOR signalling and cellular metabolism are
655 mutual determinants in cancer. *Nat. Rev. Cancer* **18**, 744–757 (2018).
656 26. Sun, Q. *et al.* Mammalian target of rapamycin up-regulation of pyruvate kinase isoenzyme
657 type M2 is critical for aerobic glycolysis and tumor growth. *Proc. Natl. Acad. Sci. U. S. A.*
658 **108**, 4129–4134 (2011).
659 27. Huye, L. E. *et al.* Combining mTor inhibitors with rapamycin-resistant T cells: A two-
660 pronged approach to tumor elimination. *Mol. Ther.* **19**, 2239–2248 (2011).
661 28. Micklethwaite, K. P. *et al.* Investigation of product-derived lymphoma following infusion
662 of piggyBac-modified CD19 chimeric antigen receptor T cells. *Blood* **138**, 1391–1405
663 (2021).
664 29. Bishop, D. C. *et al.* Development of CAR T-cell lymphoma in 2 of 10 patients effectively
665 treated with piggyBac-modified CD19 CAR T cells. *Blood* **138**, 1504–1509 (2021).
666 30. Chi, H. Regulation and function of mTOR signalling in T cell fate decisions. *Nat. Rev.*
667 *Immunol.* **12**, 325–338 (2012).
668 31. Erwood, S. *et al.* Saturation variant interpretation using CRISPR prime editing. *Nat.*
669 *Biotechnol.* **40**, 885–895 (2022).
670 32. Levesque, S. *et al.* Marker-free co-selection for successive rounds of prime editing in
671 human cells. *Nat. Commun.* **13**, 5909 (2022).
672 33. Wright, B. W., Molloy, M. P. & Jaschke, P. R. Overlapping genes in natural and
673 engineered genomes. *Nat. Rev. Genet.* **23**, 154–168 (2021).
674 34. Wagle, N. *et al.* Response and acquired resistance to everolimus in anaplastic thyroid
675 cancer. *N. Engl. J. Med.* **371**, 1426–1433 (2014).
676 35. Lorenz, M. C. & Heitman, J. TOR mutations confer rapamycin resistance by preventing
677 interaction with FKBP12-rapamycin. *J. Biol. Chem.* **270**, 27531–27537 (1995).
678 36. Rodrik-Outmezguine, V. S. *et al.* Overcoming mTOR resistance mutations with a new-
679 generation mTOR inhibitor. *Nature* **534**, 272–276 (2016).
680 37. Choi, J., Chen, J., Schreiber, S. L. & Clardy, J. Structure of the FKBP12-rapamycin
681 complex interacting with the binding domain of human FRAP. *Science* **273**, 239–242

682 (1996).
683 38. Oki, T. *et al.* Imaging dynamic mTORC1 pathway activity in vivo reveals marked shifts
684 that support time-specific inhibitor therapy in AML. *Nat. Commun.* **12**, 245 (2021).
685 39. Nelson, J. W. *et al.* Engineered pegRNAs improve prime editing efficiency. *Nat.*
686 *Biotechnol.* **40**, 402–410 (2021).
687 40. Chresta, C. M. *et al.* AZD8055 is a potent, selective, and orally bioavailable ATP-
688 competitive mammalian target of rapamycin kinase inhibitor with in vitro and in vivo
689 antitumor activity. *Cancer Res.* **70**, 288–298 (2010).
690 41. Concordet, J. P. & Haeussler, M. CRISPOR: Intuitive guide selection for CRISPR/Cas9
691 genome editing experiments and screens. *Nucleic Acids Res.* **46**, 242–245 (2018).
692 42. Vakulskas, C. A. *et al.* A high-fidelity Cas9 mutant delivered as a ribonucleoprotein
693 complex enables efficient gene editing in human hematopoietic stem and progenitor cells.
694 *Nat. Med.* **24**, 1216–1224 (2018).
695 43. Tsai, S. Q. *et al.* GUIDE-seq enables genome-wide profiling of off-target cleavage by
696 CRISPR-Cas nucleases. *Nat. Biotechnol.* **33**, 187–198 (2015).
697 44. Malinin, N. L. *et al.* Defining genome-wide CRISPR–Cas genome-editing nuclease
698 activity with GUIDE-seq. *Nat. Protoc.* **16**, 5592–5615 (2021).
699 45. Roth, T. L. *et al.* Reprogramming human T cell function and specificity with non-viral
700 genome targeting. *Nature* **559**, 405–409 (2018).
701 46. Leung, W.-H. *et al.* Sensitive and adaptable pharmacological control of CAR T cells
702 through extracellular receptor dimerization. *JCI Insight* **4**, e124430 (2019).
703 47. Mahalati, K. & Kahan, B. D. Clinical pharmacokinetics of sirolimus. *Clin.*
704 *Pharmacokinet.* **40**, 573–585 (2001).
705 48. Araki, K. *et al.* mTOR regulates memory CD8 T-cell differentiation. *Nature* **460**, 108–112
706 (2009).
707 49. Dormond, O., Romero, P., Zhang, L. & Romero, P. Modulation of mTOR signalling
708 triggers the formation of stem cell-like memory T cells. *EBioMedicine* **4**, 50–61 (2016).
709 50. Long, A. H. *et al.* 4-1BB costimulation ameliorates T cell exhaustion induced by tonic
710 signaling of chimeric antigen receptors. *Nat. Med.* **21**, 581–590 (2015).
711 51. Philipson, B. I. *et al.* 4-1BB costimulation promotes CAR T cell survival through
712 noncanonical NF-kB signaling. *Sci. Signal.* **13**, eaay8248 (2020).

713 52. Cappell, K. M. & Kochenderfer, J. N. A comparison of chimeric antigen receptors
714 containing CD28 versus 4-1BB costimulatory domains. *Nat. Rev. Clin. Oncol.* **18**, 715–
715 727 (2021).
716 53. Bloemberg, D. *et al.* A high-throughput method for characterizing novel chimeric antigen
717 receptors in Jurkat cells. *Mol. Ther. - Methods Clin. Dev.* **16**, 238–254 (2020).
718 54. Muller, Y. D. *et al.* The CD28-transmembrane domain mediates chimeric antigen receptor
719 heterodimerization with CD28. *Front. Immunol.* **12**, 639818 (2021).
720 55. Majzner, R. G. & Mackall, C. L. Clinical lessons learned from the first leg of the CAR T
721 cell journey. *Nat. Med.* **25**, 1341–1355 (2019).
722 56. Wu, C. Y., Roybal, K. T., Puchner, E. M., Onuffer, J. & Lim, W. A. Remote control of
723 therapeutic T cells through a small molecule-gated chimeric receptor. *Science* **350**,
724 aab4077 (2015).
725 57. Flugel, C. L. *et al.* Overcoming on-target, off-tumour toxicity of CAR T cell therapy for
726 solid tumours. *Nat. Rev. Clin. Oncol.* **20**, 49–62 (2023).
727 58. Shah, N. N. & Fry, T. J. Mechanisms of resistance to CAR T cell therapy. *Nat. Rev. Clin.*
728 *Oncol.* **16**, 372–385 (2019).
729 59. Fry, T. J. *et al.* CD22-targeted CAR T cells induce remission in B-ALL that is naive or
730 resistant to CD19-targeted CAR immunotherapy. *Nat. Med.* **24**, 20–28 (2018).
731 60. Chang, C. H. *et al.* Metabolic competition in the tumor microenvironment is a driver of
732 cancer progression. *Cell* **162**, 1229–1241 (2015).
733 61. McGuirk, S., Audet-Delage, Y. & St-Pierre, J. Metabolic fitness and plasticity in cancer
734 progression. *Trends in Cancer* **6**, 49–61 (2020).
735 62. Agudelo, D. *et al.* Marker-free coselection for CRISPR-driven genome editing in human
736 cells. *Nat. Methods* **14**, 615–620 (2017).
737 63. Grabiner, B. C. *et al.* A diverse array of cancer-associated MTOR mutations are
738 hyperactivating and can predict rapamycin sensitivity. *Cancer Discov.* **4**, 554–563 (2014).
739 64. Wagle, N. *et al.* Activating mTOR mutations in a patient with an extraordinary response
740 on a phase I trial of everolimus and pazopanib. *Cancer Discov.* **4**, 546–553 (2014).
741 65. Gumber, D. & Wang, L. D. Improving CAR-T immunotherapy: Overcoming the
742 challenges of T cell exhaustion. *eBioMedicine* **77**, 103941 (2022).
743 66. Mestermann, K. *et al.* The tyrosine kinase inhibitor dasatinib acts as a pharmacologic

744 on/off switch for CAR T cells. *Sci. Transl. Med.* **11**, eaau5907 (2019).
745 67. Weber, E. W. *et al.* Pharmacologic control of CAR-T cell function using dasatinib. *Blood*
746 *Adv.* **3**, 711–717 (2019).
747 68. Weber, E. W. *et al.* Transient rest restores functionality in exhausted CAR-T cells through
748 epigenetic remodeling. *Science* **372**, eaba1786 (2021).
749 69. Fajgenbaum, D. C. & June, C. H. Cytokine storm. *N. Engl. J. Med.* **383**, 2255–2273
750 (2020).
751 70. Morris, E. C., Neelapu, S. S., Giavridis, T. & Sadelain, M. Cytokine release syndrome and
752 associated neurotoxicity in cancer immunotherapy. *Nat. Rev. Immunol.* **22**, 85–96 (2022).
753 71. Alizadeh, D. *et al.* IL15 enhances CAR-T cell antitumor activity by reducing mTORC1
754 activity and preserving their stem cell memory phenotype. *Cancer Immunol. Res.* **7**, 759–
755 772 (2019).
756 72. Lamarthée, B. *et al.* Transient mTOR inhibition rescues 4-1BB CAR-Tregs from tonic
757 signal-induced dysfunction. *Nat. Commun.* **12**, 6446 (2021).
758 73. Chen, P. J. *et al.* Enhanced prime editing systems by manipulating cellular determinants of
759 editing outcomes. *Cell* **184**, 5635–5652 (2021).
760 74. Nguyen, D. N. *et al.* Polymer-stabilized Cas9 nanoparticles and modified repair templates
761 increase genome editing efficiency. *Nat. Biotechnol.* **38**, 44.49 (2019).
762 75. Brinkman, E. K., Chen, T., Amendola, M. & Van Steensel, B. Easy quantitative
763 assessment of genome editing by sequence trace decomposition. *Nucleic Acids Res.* **42**,
764 e168 (2014).
765 76. Brinkman, E. K. *et al.* Easy quantification of template-directed CRISPR/Cas9 editing.
766 *Nucleic Acids Res.* **46**, e58 (2018).
767 77. Xu, L., Liu, Y. & Han, R. BEAT: A Python program to quantify base editing from Sanger
768 sequencing. *Cris. J.* **2**, 223–229 (2019).
769 78. Clement, K. *et al.* CRISPResso2 provides accurate and rapid genome editing sequence
770 analysis. *Nat. Biotechnol.* **37**, 215–226 (2019).
771 79. Bloh, K. *et al.* Deconvolution of complex DNA repair (DECODR): establishing a novel
772 deconvolution algorithm for comprehensive analysis of CRISPR-edited Sanger
773 sequencing data. *Cris. J.* **4**, 120–131 (2021).
774 80. Hamieh, M. *et al.* CAR T cell trogocytosis and cooperative killing regulate tumour antigen

escape. *Nature* **568**, 112–116 (2019).

ACKNOWLEDGEMENTS

This study was supported by a grant from Mitacs and by the Fondation du CHU de Québec. JJ. L. is supported by a CIHR Project Grant (PJT407274). S.L. was supported by a Frederick Banting and Charles Best Canada graduate scholarship from CIHR, and a Graduate student scholarship from the Fonds de la Recherche du Québec-Santé (FRQS). G.C. holds a Vanier Canada graduate scholarship from CIHR. Salary support was provided by the FRQS to Y.D. B.B. and G.M. are supported by the "Programme d'appui aux plateformes technologiques stratégiques" from the Ministère de l'Économie, de l'Innovation et de l'Énergie Québec. We thank the staff at the flow cytometry core facility of the CHU de Quebec Research Center for their training and assistance. We thank Marie-Ève Paquet and the vector core facility staff at the Canadian neurophotonics platform for AAV6 production. We also thank Scott McComb (National Research Council) for kindly providing NALM6-RFP-FLUC cells.

COMPETING INTERESTS

S.L. and Y.D. are co-inventors on a patent application (WO 2023/015376 A1) related to this work.

AUTHOR'S CONTRIBUTIONS

Conceptualization, S.L. and Y.D.; methodology, S.L., G.C., V.D., C.G., JP. F., S.V., E.N., G.M., N.D., J.L., B.B., JJ. L., and Y.D.; investigation, S.L., G.C., V.D., C.G., JP. F., S.V., E.N., G.M., N.D., J.L., B.B., JJ. L., and Y.D.; writing original draft, S.L.; writing, review and editing, S.L., and Y.D.; supervision, J.L., B.B., JJ. L., and Y.D.; funding acquisition, J.L., JJ. L., and Y.D. All authors reviewed the manuscript and approved its final version.

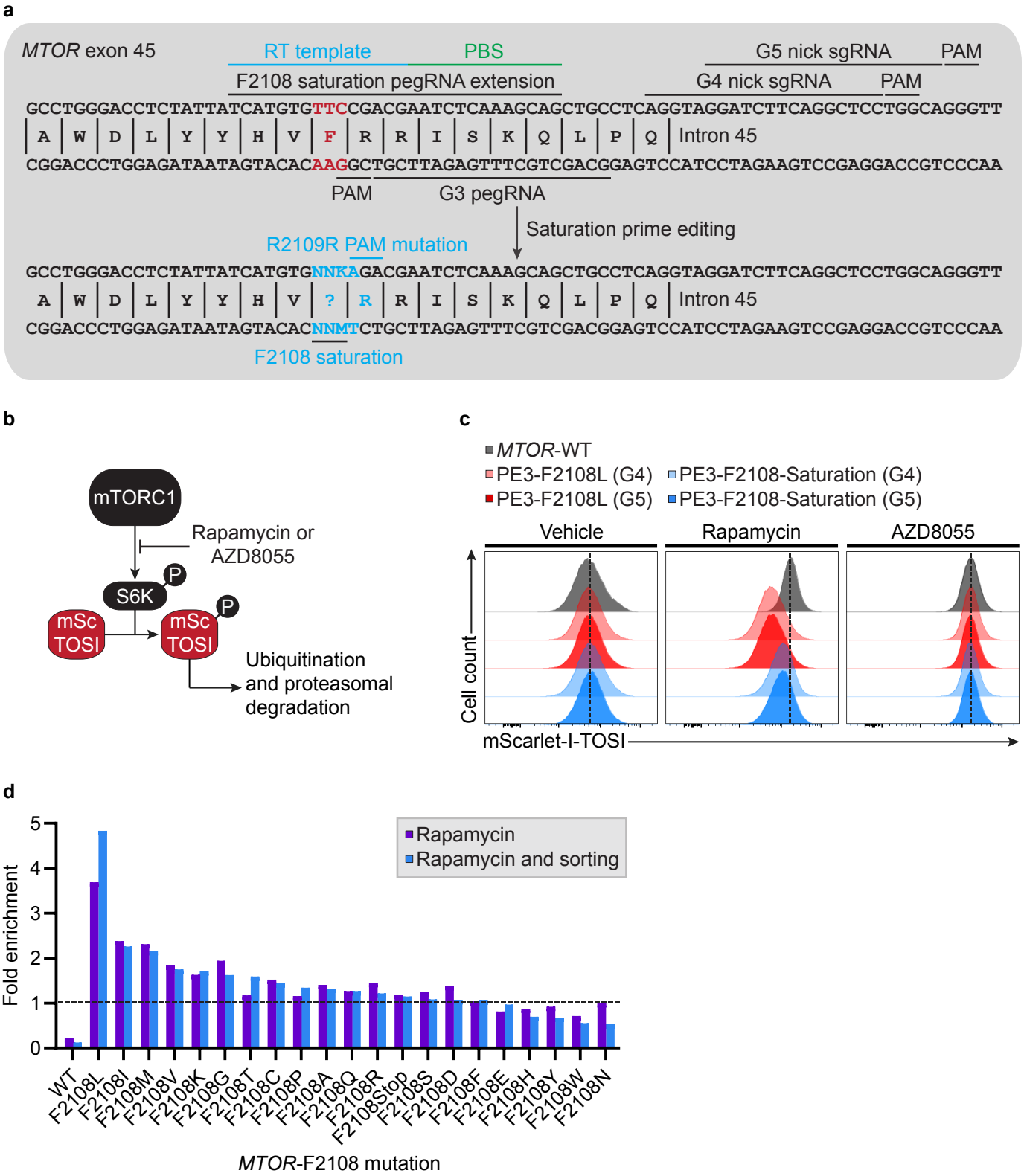

Figure 1
Levesque et al.

801 **Figure 1. Identification of mutations conferring rapamycin resistance via saturation prime**
802 **editing.** (**a**) Schematic representation of the SpCas9 target sites, the reverse transcriptase (RT)
803 template and the primer binding site (PBS) used to perform genome editing at *MTOR*. To perform
804 saturation prime editing, G3 is used as a pegRNA, and G4 or G5 are used as a complementary nick
805 sgRNA (PE3). The *MTOR*-F2108 codon is mutated to NNK and an additional silent PAM mutation
806 is introduced. (**b**) Schematic of mScarlet-I mTOR signaling indicator (mSc-TOSI) degradation
807 under mTORC1 signaling. (**c**) Histogram plot of mSc-TOSI intensity in bulk populations of cells
808 harboring different *MTOR*-F2108 mutations. Where indicated, cells were treated for 24 hours with
809 50 nM rapamycin or 50 nM AZD8055 before FACS analysis. Representative images are from one
810 of two independent biological replicates performed at different times with equivalent results. (**d**)
811 High throughput sequencing quantification of the *MTOR*-F2108 mutations introduced via
812 saturation prime editing following rapamycin selection and FACS sorting. The fold enrichment of
813 each *MTOR*-F2108 mutation was calculated from the before selection sample.

a

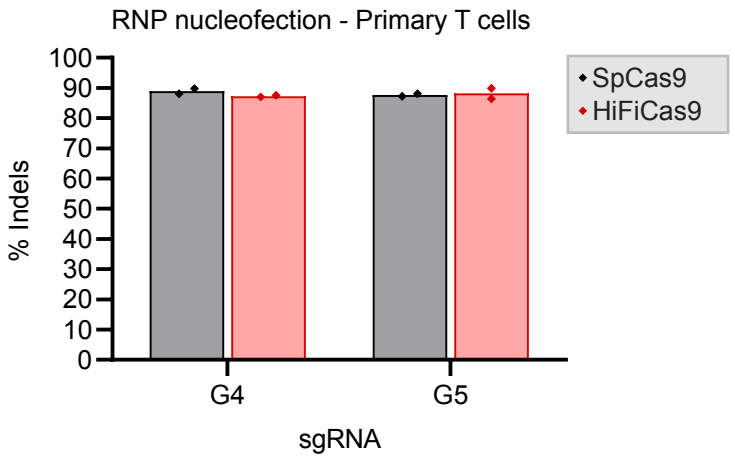

b

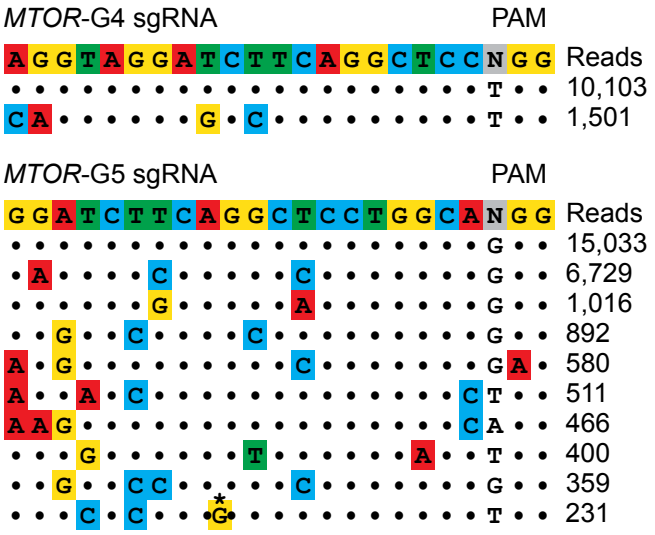

Figure 2
Levesque et al.

814 **Figure 2. Identification of highly active and specific sgRNAs targeting the *MTOR* locus.** (**a**)
815 Small indels quantification as determined by TIDE analysis from Sanger sequencing. Primary
816 $CD3^+$ and $CD8^+$ T cells were transfected with the indicated nuclease/sgRNA RNPs and genomic
817 DNA was harvested 3 days post-transfection. $n = 2$ independent biological replicates performed at
818 different times with $CD3^+$ and $CD8^+$ T cells from two different healthy donors. (**b**) Candidate off-
819 target sites identified using GUIDE-Seq. $CD3^+$ T cells were transfected with SpCas9 RNPs
820 targeting *MTOR* intron 45 and GUIDE-Seq dsDNA. Four days post-nucleofection, $CD3^+$ T cells
821 were restimulated and expanded for an additional 7 days. Genomic DNA was harvested after
822 expansion (11 days post-nucleofection). Dots represent matches with the intended target sequence,
823 mismatches are colored, and nucleotide bulges are highlighted with a star. GUIDE-Seq read counts
824 are from one of two independent biological replicates performed with $CD3^+$ T cells from two
825 different donors (see **Supplementary Fig. 3**).
826

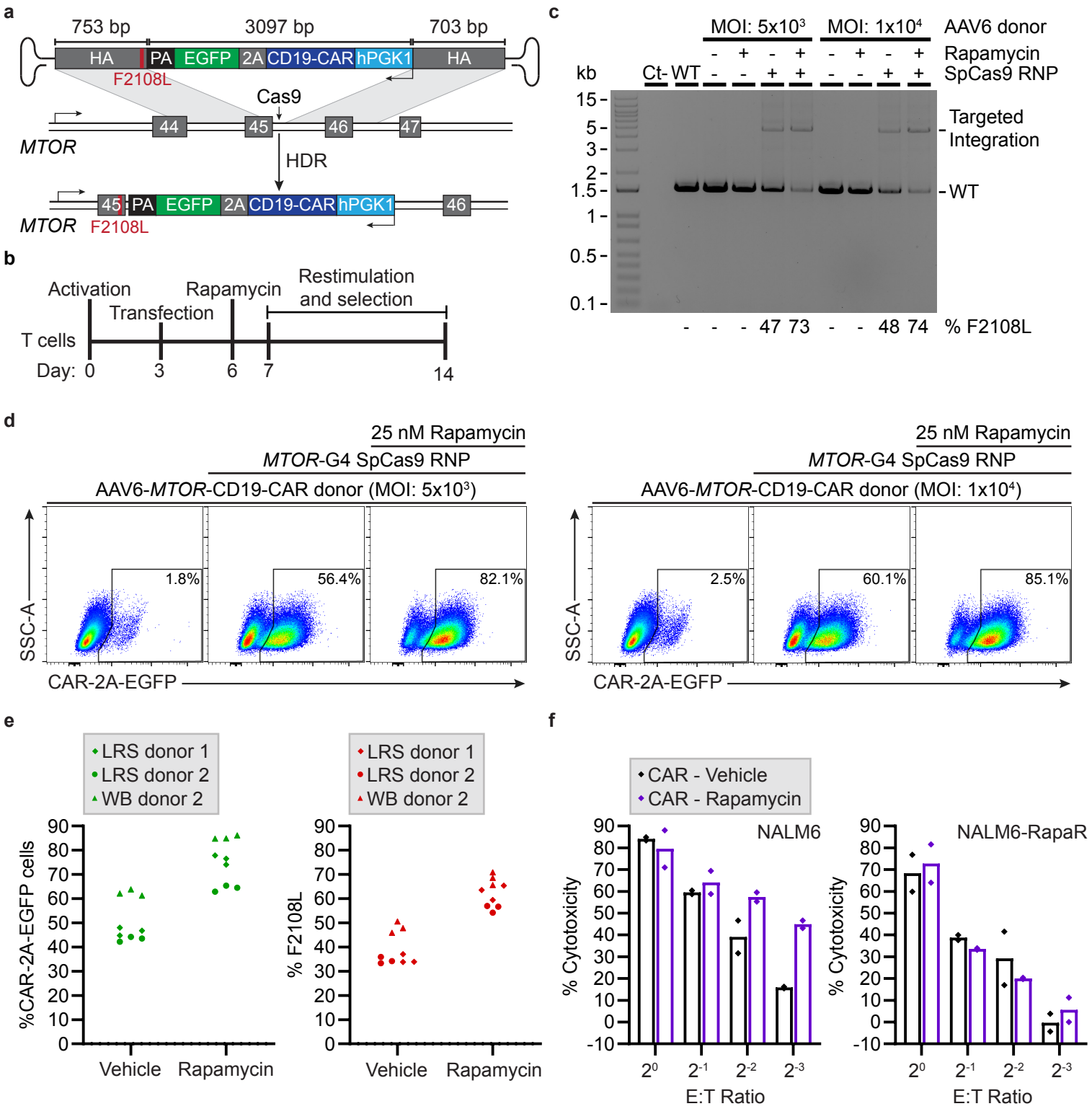

Figure 3
Levesque et al.

827 **Figure 3. Targeting a CAR to the *MTOR* locus allows the enrichment of rapamycin-resistant**
828 **CAR-T cells.** (**a**) Schematic representation of CD19-CAR-2A-EGFP targeting to the reverse DNA
829 strand of the *MTOR* locus using an AAV6 donor. The F2108L mutation is introduced via the left
830 homology arm (HA) and transgene expression is driven by a human *PGK1* promoter. (**b**)
831 Representative timeline for nucleofection and *ex vivo* rapamycin selection. (**c**) Out-Out PCR for
832 CD19-CAR-2A-EGFP knock-in detection at *MTOR*. Whole blood (WB) primary $CD3^+$ T cells
833 from WB donor 1 (WB 1) were transfected with a SpCas9-G4 RNP and transduced with an AAV6
834 vector with the indicated multiplicity of infection (MOI). T cells were treated (rapamycin) or not
835 (vehicle) with 25 nM rapamycin 3 days post-transfection for 8 days. The percentage of edited
836 alleles was determined by TIDER from Sanger sequencing. $n = 1$ experiment. (**d**) Same as in (**c**),
837 but FACS-based quantification of targeted CD19-CAR-2A-EGFP integration. (**e**) Same as in (**c,d**)
838 with a MOI of $5x10^3$ and primary $CD3^+$ T cells isolated from WB or a leukocyte reduction system
839 (LRS) from three additional healthy donors. $n = 3$ independent biological replicates performed in
840 triplicate at different times with $CD3^+$ T cells from the indicated healthy donor. Each data point
841 represents a technical replicate. (**e**) Luciferase-based cytotoxicity assay. Following rapamycin
842 selection, CD19-CAR-T cells were incubated with the indicated effector to target (E:T) ratio with
843 NALM6 cells stably expressing firefly luciferase (FLUC) and 25 nM rapamycin. Rapamycin-
844 resistant NALM6 cells harboring the *MTOR*-F2108L mutation (NALM6-RapaR) were used as a
845 control to analyze the combinatorial impact of rapamycin. Luminescence was measured after 18
846 hours of incubation. $n = 2$ independent biological replicates performed at different times with $CD3^+$
847 T cells from two different healthy donors (WB donor 1 and LRS donor 2). Each data point
848 represents the average of three technical replicates. *hPGK1*, human phosphoglycerate kinase 1
849 promoter. PA, polyadenylation signal. HA, homology arm.
850

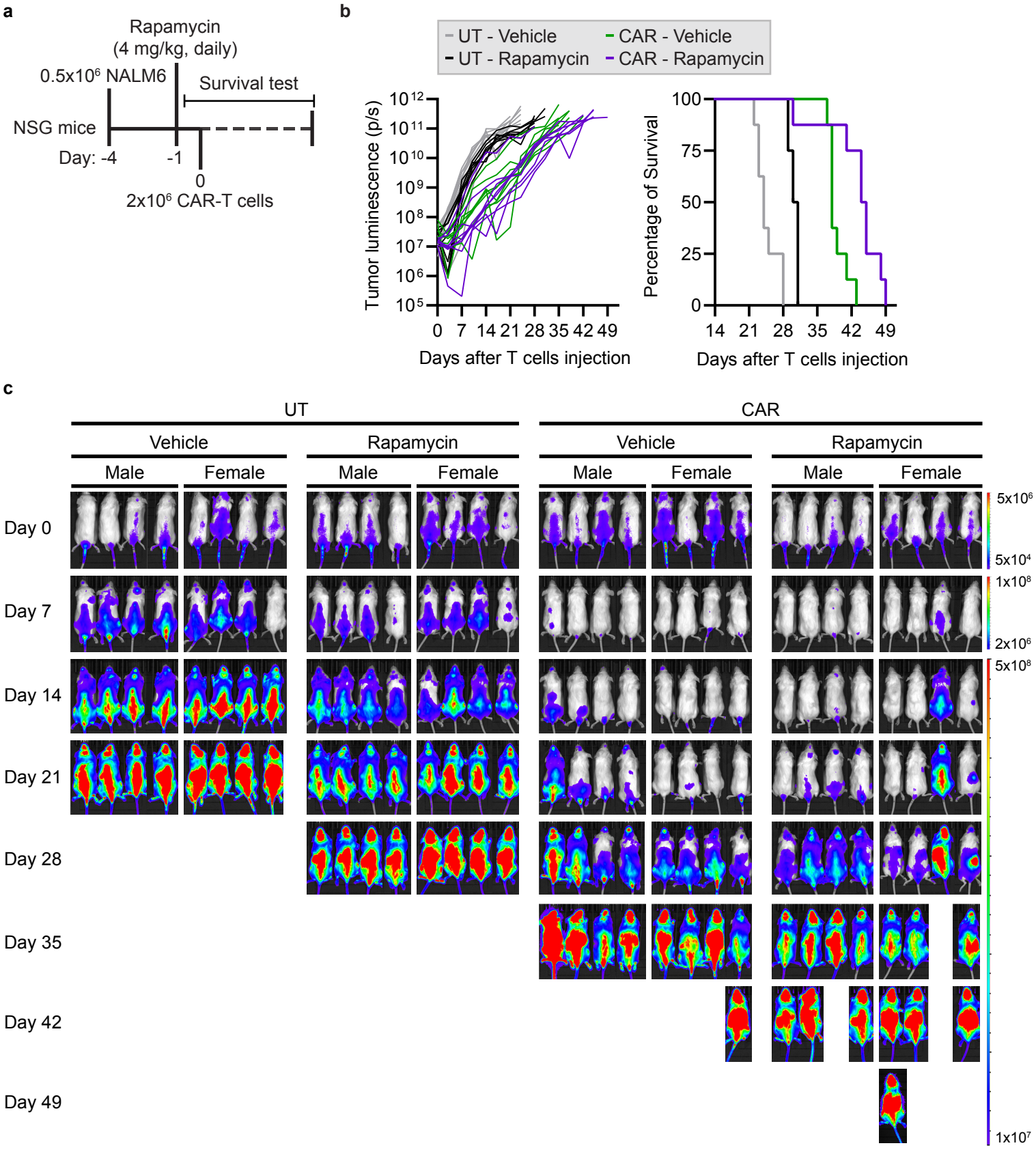

Figure 4
Levesque et al.

851 **Figure 4. Combinatorial CAR-T cell therapy with rapamycin slows leukemia progression *in***
852 ***vivo*.** (**a**) Timeline and experimental setup for the pre-B acute lymphoblastic leukemia xenograft
853 mouse model. Male and female NSG mice were challenged with 0.5 x 10^5 NALM6-RFP-FLUC
854 cells and daily rapamycin treatment (4 mg/kg) started three days later. Four days after tumor
855 inoculation, 2 x 10^6 untransduced (UT) T cells or CD19-CAR-T cells were injected (Donor ID
856 WB2, see **Fig. 3e**). (**b**) Bioluminescence (BLI) quantification and Kaplan-Meier survival plot.
857 Leukemia engraftment, bio-distribution, and tumor progression were assessed by BLI imaging two
858 times per week. The radiance (photons/s) of the regions of interest (ROIs) corresponds to the area
859 containing the whole back side of the body. n = 8 mice per group. (**c**) BLI and tumor bio-
860 distribution of all mice from (**b**) over seven weeks. The color barcode represents the radiance scale
861 (photons/s/cm^2/sr).
862

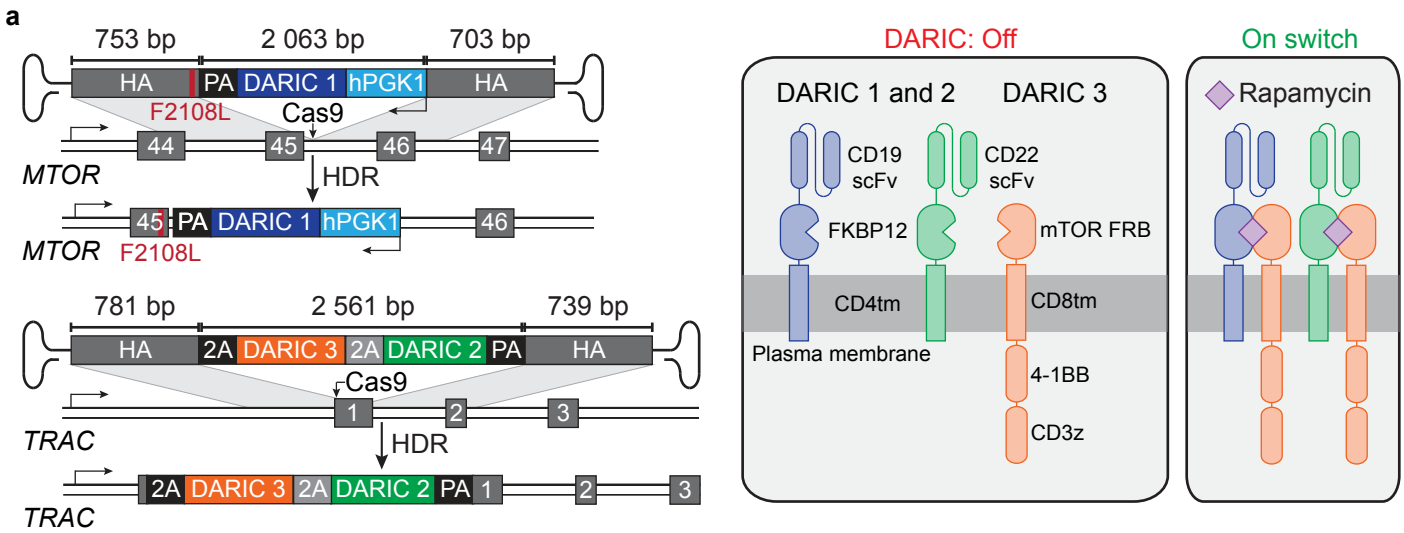
a
753 bp
2 063 bp
703 bp
HA
PA
DARIC 1
hPGK1
HA
F2108L
Cas9
44
45
46
47
MTOR
HDR
45
PA
DARIC 1
hPGK1
46
MTOR
F2108L
781 bp
2 561 bp
739 bp
HA
2A
DARIC 3
2A
DARIC 2
PA
HA
Cas9
1
2
3
TRAC
HDR
2A
DARIC 3
2A
DARIC 2
PA
1
2
3
TRAC
DARIC: Off
On switch
DARIC 1 and 2
DARIC 3
Rapamycin
CD19 scFv
CD22 scFv
FKBP12
mTOR FRB
CD4tm
CD8tm
Plasma membrane
4-1BB
CD3z

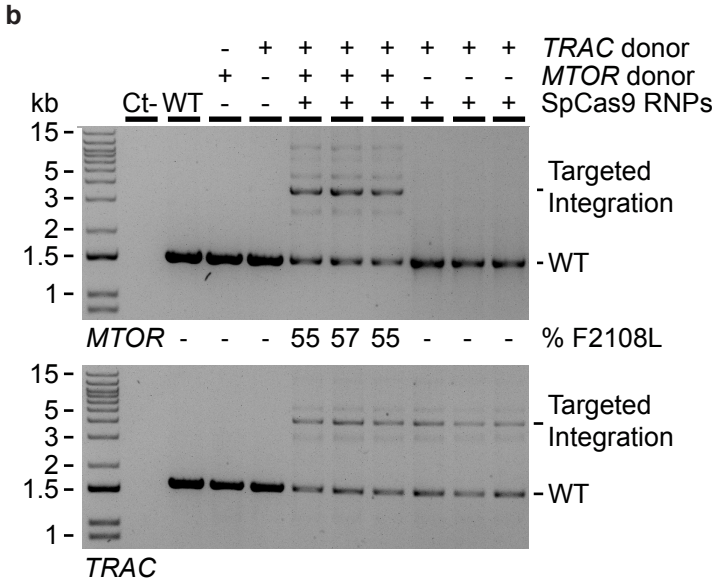
b
TRAC donor
MTOR donor
SpCas9 RNPs
kb
Ct-
WT
15
5
3
2
1.5
1
Targeted Integration
WT
MTOR
55 57 55
% F2108L
TRAC

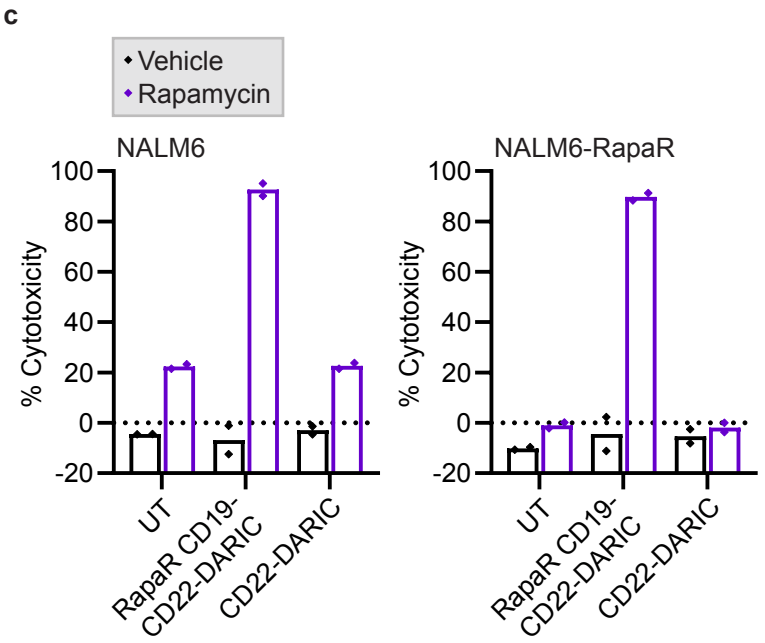
c
Vehicle
Rapamycin
NALM6
NALM6-RapaR
% Cytotoxicity
100
80
60
40
20
0
-20
UT
RapaR CD19-CD22-DARIC
CD22-DARIC

863 **Figure 5. Multiplexed DARIC targeting to the *MTOR* and *TRAC* loci allows pharmacological**
864 **control of CAR-T cells activity.** (**a**) Schematic representation of DARIC-1 targeting to the reverse
865 DNA strand of the *MTOR* locus, and DARIC-2 and 3 targeting to the *TRAC* locus using AAV6
866 donors. (**b**) Out-Out PCR for DARIC-1 knock-in detection at *MTOR* and DARIC-2 and 3 knock-
867 in at *TRAC*. Whole blood (WB) primary $CD3^+$ T cells were transfected with a SpCas9-G4 RNP
868 and transduced with AAV6 vectors with a multiplicity of infection (MOI) of $5x10^3$ for each AAV6.
869 Genomic DNA was harvested 3 days post-transfection. The percentage of edited alleles was
870 determined by TIDER from Sanger sequencing. Representative images are from one of two
871 independent biological replicates. (**c**) FACS-based cytotoxicity assay. $CD3^+$ T cells were
872 electroporated with *MTOR*/*TRAC* RNPs and transduced with both *MTOR*/*TRAC* AAV6 donors to
873 generate rapamycin-resistant (RapaR) CD19-CD22-DARIC-T cells. For rapamycin-sensitive
874 CD22-DARIC-T cells, the *MTOR* AAV6 donor was omitted. Three days post-nucleofection,
875 DARIC-T cells were incubated in the presence (rapamycin) or absence (vehicle) of 25 nM
876 rapamycin with NALM6 cells stably expressing RFP and K562-RapaR stably expressing EBFP
877 with an effector to target ratio of 1:1. Rapamycin-resistant NALM6 cells harboring the *MTOR*-
878 F2108L mutation (NALM6-RapaR) were used as a control to analyze the combinatorial impact of
879 rapamycin. The percentage of cytotoxicity was measured by FACS after 72 hours of incubation. *n*
880 = 2 independent biological replicates. Each data point represents the average of three technical
881 replicates.